

primary cancer and tumor location in the eloquent cortex were significantly associated with complications. However, no chronological data were presented in their article, and there was no description of delayed complications. Varlotto et al reported (11) that among 137 patients with brain metastases who survived for at least 1 year after GKRS, postradiosurgical sequelae developed in 2.8% and 11.4% of patients at the first and fifth year, respectively, after GKRS. The incidence of 11.4% at the fifth post-GKRS year was far higher than our result, 4.2%. In their study, only the standard Kaplan-Meier method was used. This method assumes that follow-up of those developing a competing event (death) is simply censored. We consider competing risk analysis to have been necessary for evaluation of their data (6, 7). Furthermore, their Kaplan-Meier plot of the proportion without neurologic sequelae showed that none of their patients experienced neurologic sequelae between the 24th and 120th post-GKRS months. In other words, Varlotto et al (11) observed complications that occurred in a somewhat earlier post-GKRS period, 2 years or less. By contrast, herein we have described delayed complications occurring 24 months or more after GKRS, and our data demonstrated a time-related increase in the incidence (Fig. 1).

### Predictive factors

Several authors have shown correlations with tumor volume and/or WBRT and complications (11, 14–17). In our present study, the only factor associated with delayed complications was larger tumor volume. Nakagawa et al reported prior or concomitant WBRT to be a possible risk factor for low-grade dementia (16). We also observed 1 patient in whom severe dementia occurred after WBTR followed by GKRS (8). However, in our series, a small number of patients—only 4—underwent WBRT, so the correlation between WBRT and delayed complications was unclear. It is common knowledge in radiobiology that higher irradiation doses carry a higher risk of complications. The median peripheral dose, 24.0 Gy, in the subset reported here was higher than the 21.0 Gy in our entire cohort (2000 cases). We cannot deny that such a relatively high dose may have an impact on delayed complications, although univariate analysis did not demonstrate the peripheral dose to be a predictive factor for delayed complications in this study (Table 3).

Paddick and Lippitz (10) found, among several radiosurgical parameters, the gradient index to be a crucial factor for complication avoidance. Also, Ishikawa et al (3) described, as noted in our previous report on delayed cyst formation after GKRS for patients with brain metastases, that a poor gradient index may partially explain the observed phenomenon. However, univariate analysis did not demonstrate the gradient index to be a predictive factor for delayed complications in this study. Although Varlotto et al (11) found that complications correlated with brain volume receiving  $\geq 12$  Gy and we reported receiving  $\geq 5$  Gy to be important (12), neither  $\geq 12$  Gy nor  $\geq 5$  Gy irradiated brain volume was associated with delayed complications in our present study.

### Pathogenesis

The first author (M.Y.) previously reported post-GKRS sequelae (ie, expanding mass lesions with or without cyst formation) occurring many years after GKRS for arteriovenous malformations (18, 19). Our present study revealed similar complications to occur in long-term survivors after GKRS for brain metastases. As noted in our

previous report, the mechanism of delayed cyst formation after GKRS for brain metastases is speculated to be increased permeability through partially injured blood vessel walls within the degenerated or scar tissue (3). However, the mechanism of enhanced mass lesions has yet to be fully elucidated. The histopathologic changes of resected specimens in the 6 cases reported herein were characterized as degenerated tissue mainly consisting of fibrous tissue and various stages of hemorrhage, from fresh to organized with hemosiderin deposits. Also, there was evidence of neovascularization, enlarged vessels, and albuminous fluid exudation. In most cases, the irradiated metastatic lesions showed findings from coagulation necrosis to liquefaction necrosis and ultimately collapsed, as Szeifert et al very recently described (20). However, we speculate that in some other cases, degenerated tissue remains for many years and reparative processes may occur after repeated intranidal microhemorrhage, which may finally cause an expanding mass lesion, although the triggering mechanism remains unknown. Therefore, the existence of a long-standing enhanced area may be a risk factor for delayed complications.

### Treatment

Observation alone is reasonable for compensated and asymptomatic patients because spontaneous regression can be expected in some, as is the case in patients with arteriovenous malformations. When delayed cysts and/or enhanced mass lesions are symptomatic, surgical intervention should be considered. Even if these conditions have not yet produced neurologic symptoms, surgical intervention is recommended for patients whose cysts and/or mass lesions show continuous expansion. For a patient with a simple cyst, we believe that Ommaya reservoir placement may be a better choice than fluid aspiration without a reservoir, because some patients require reaspiration. Moreover, Ommaya tube placement may maintain the drainage tract from the cyst to the subarachnoid space, thereby preventing cyst regrowth. For a patient with an enhanced mass lesion with or without cyst formation, however, surgical resection should be considered even if the mass lesion is not particularly large. In any case, the surgical results of our present series were favorable.

### Conclusions

In conclusion, 10.2% of long-surviving patients showed delayed complications, with a median interval of 53 months (range, 24.0–121.0 months) after GKRS for brain metastases. A larger tumor volume, particularly larger than 10 cc, was a risk factor for these complications. Long-term follow-up is crucial for patients with brain metastases treated with GKRS because the risk of complications long after treatment is not insignificant. However, if a delayed complication does occur, a favorable outcome can be expected with timely surgical intervention. This is considered to be quite different from WBRT, which causes the untreatable complication of decreased NCF.

### References

1. Linskey ME, Andrews DW, Asher AL, et al. The role of stereotactic radiosurgery in the management of patients with newly diagnosed brain metastases: a systematic review and evidence-based clinical practice guideline. *J Neurooncol* 2010;96:45-68.

2. McDermott MW, Sneed PK. Radiosurgery in metastatic brain cancer. *Neurosurgery* 2005;57(Suppl S4):45-53.
3. Ishikawa E, Yamamoto M, Saito A, et al. Delayed cyst formation after gamma knife radiosurgery for brain metastases. *Neurosurgery* 2009;65:689-695.
4. Radiation Therapy Oncology Group Cooperative Group Common Toxicity Criteria. <http://www.rtog.org/ResearchAssociates/AdverseEventReporting.aspx>. Accessed September 30, 2011.
5. Gasper L, Scott C, Rotman M, et al. Recursive partitioning analysis (RPA) of prognostic factors in three Radiation Therapy Oncology Group (RTOG) brain metastases trials. *Int J Radiat Oncol Biol Phys* 1997;37:745-751.
6. Gooley TA, Leisenring W, Crowley J, et al. Estimation of failure probabilities in the presence of competing risks: new representations of old estimators. *Stat Med* 1999;18:695-706.
7. Fine JP, Gray RJ. A proportional hazards model for the subdistribution of a competing risk. *J Am Stat Assoc* 1999;94:496-509.
8. Yamamoto M. Radiosurgery for metastatic brain tumors. *Prog Neurol Surg* 2007;20:106-128.
9. Paddick I. A simple scoring ratio to index the conformity of radio-surgical treatment plans. *J Neurosurg* 2000;93(Suppl):219-222.
10. Paddick I, Lippitz B. A simple dose gradient measurement tool to complement the conformity index. *J Neurosurg* 2006;105(Suppl):194-201.
11. Varlotto JM, Flickinger JC, Niranjan A, et al. Analysis of tumor control and toxicity in patients who have survived at least one year after radiosurgery for brain metastases. *Int J Radiat Oncol Biol Phys* 2003;57:452-464.
12. Yamamoto M, Ide M, Nishio S, et al. Gamma knife radiosurgery for numerous brain metastases: is this a safe treatment? *Int J Radiat Oncol Biol Phys* 2002;53:1279-1283.
13. Yamamoto M, Kawabe T, Bierta E, et al. How many metastases can be treated with radiosurgery? *Prog Neurol Surg* 2012;26:261-272.
14. Williams BJ, Suki D, Fox BD, et al. Stereotactic radiosurgery for metastatic brain tumors: a comprehensive review of complications. *J Neurosurg* 2009;111:439-448.
15. Joseph J, Adler JR, Cox RS, et al. Linear accelerator-based stereotaxic radiosurgery for brain metastases: the influence of number of lesions on survival. *J Clin Oncol* 1996;14:1085-1092.
16. Nakagawa K, Tago M, Terahara A, et al. A single institutional outcome analysis of gamma knife radiosurgery for single or multiple brain metastases. *Clin Neurol Neurosurg* 2000;102:227-232.
17. Shiau CY, Sneed PK, Shu H, et al. Radiosurgery for brain metastases: relationship of dose and pattern of enhancement to local control. *Int J Radiat Oncol Biol* 1997;37:375-383.
18. Yamamoto M, Jimbo M, Hara M, et al. Gamma knife radiosurgery for arteriovenous malformations: long-term follow-up results focusing on complications occurring more than five years after irradiation. *Neurosurgery* 1996;38:906-914.
19. Yamamoto M, Hara M, Ide M, et al. Radiation-related adverse effects observed on neuro-imaging several years after radiosurgery for cerebral arteriovenous malformations. *Surg Neurol* 1998;49:387-398.
20. Szeifert GT, Kondziolka D, Lunsford LD, et al. The contribution of pathology to radiosurgery. *Prog Neurol Surg* 2007;20:1-15.

## Analysis of progression and recurrence of meningioma using $^{11}\text{C}$ -methionine PET

Hidetoshi Ikeda · Naohiro Tsuyuguchi ·  
Noritsugu Kunihiro · Kenichi Ishibashi ·  
Takeo Goto · Kenji Ohata

Received: 31 January 2013 / Accepted: 16 June 2013 / Published online: 26 June 2013  
© The Japanese Society of Nuclear Medicine 2013

### Abstract

**Objective** The recurrence rate of meningioma after surgery is high, and progression is often observed. The risk factors for recurrence and progression are not clear. We evaluated the risk factors for recurrence and progression in meningioma using  $^{11}\text{C}$ -methionine (MET) positron emission tomography (PET).

**Methods** Thirty-seven patients (mean follow-up, 80 months) with an intracranial meningioma were enrolled. MET PET was performed before treatment between 1995 and 2010, and patients were followed up in an out-patient clinic. Surgery was performed in 33 patients, and a wait-and-see approach was taken in four patients. We evaluated the extent of tumor resection, location, WHO grade, Ki-67 labeling index, and lesion to normal ratio (LN ratio) of MET uptake.

**Results** Six of the surgical cases had a recurrence, and two of the observation-only patients had tumor progression. A high LN ratio of MET uptake was a significant risk factor for recurrence and progression with univariate analysis. The area under the curve of receiver operating characteristic curve for the LN ratio of MET uptake was 0.754, and the optimal cutoff value was 3.18 (sensitivity 63 %, specificity 79 %). With multivariate analysis, a high LN ratio of MET uptake, non-gross total resection, and a high WHO grade were significant risk factors for progression and recurrence.

**Conclusion** A high LN ratio of MET uptake was a risk factor for tumor progression and recurrence. The advantage of MET PET is that it is not invasive and can easily be used to evaluate the whole tumor.

**Keywords**  $^{11}\text{C}$ -methionine PET · Meningioma · Riskfactor of recurrence and progression · Multivariable analysis · ROC analysis

### Introduction

Meningioma is the most common primary brain tumor in adults. The frequency of meningioma among all types of brain tumors is 26.4 % in Japan [1] and 34.4 % in the United States. Many histopathological subtypes exist. Most meningiomas are benign, but World Health Organization (WHO) grade II and grade III meningiomas, which exhibit aggressive clinical behavior, are found in 10 % of patients with meningioma. We usually perform surgery for symptomatic cases or cases with large tumors. For small and asymptomatic cases, a wait-and-see approach is taken. However, gross total resection (GTR) is difficult in some surgical cases because of the tumor location and invasion into the brain tissue and the venous sinus. The residual tumor often recurs with malignancy, making the patient's prognosis poor. Meningiomas that are only observed sometimes progress and require surgical resection. In previous papers, the recurrence rate after surgery was high. Even if the tumor is removed completely, the recurrence rate is between 7 and 32 %. After subtotal resection, the recurrence rate is between 19 and 50 % [2–4].

The risk factors for progression and recurrence in meningioma are not clear, and clarification of these factors is important for determining surgical indications and

H. Ikeda (✉) · N. Tsuyuguchi · N. Kunihiro · K. Ishibashi ·  
T. Goto · K. Ohata  
Department of Neurosurgery, Osaka City University Graduate  
School of Medicine, 1-4-3 Asahi-machi, Abeno-ku,  
Osaka 545-8585, Japan  
e-mail: hide-i@med.osaka-cu.ac.jp

treatment strategies. We usually use the Ki-67 labeling index (LI) to evaluate the proliferative activity, but surgery is required to obtain a tissue specimen. Surgery is invasive for the patient, and evaluating the risk of recurrence with the Ki-67 LI is controversial because the tissue specimen sometimes does not reflect the whole tumor.

In this study, we evaluated  $^{11}\text{C}$ -methionine (MET) uptake of the whole tumor using MET positron emission tomography (PET) to investigate the risk factors for recurrence and progression.

## Methods

### Patients

From a database of patients who were examined with MET PET, we retrospectively retrieved data for all 73 patients who were diagnosed with intracranial meningioma between 1995 and 2010. These cases were not a consecutive series. We could not examine MET PET results for all meningioma cases because the number of cases that could be examined by MET PET per week in our facilities is limited. Thirty-seven patients fulfilled the inclusion criteria for this study: (1) patients were initially diagnosed with meningioma; (2) MET PET was performed before surgery or observation; (3) patients were followed at Osaka City University Hospital or affiliated hospitals; (4) during the follow-up period, no additional treatment was performed other than the first surgery. Thirty-three patients were excluded because of recurrence after surgery, and three patients dropped out during the follow-up period. Thus, 37 cases (23 females and 14 males) were enrolled in this study (Fig. 1). The mean age of the patients was  $54.5 \pm 12.9$  years. All study participants provided

informed consent, and the study design was approved by an ethics review board.

### MET PET study

All patients underwent a MET PET scan with HEADTOME-IV (BGO, Shimadzu, Japan) between 1995 and 2005, Eminence-B (BGO) since 2005, and Biograph-16 (LSO, Siemens, Germany) since 2010. Twenty-six patients were examined with HEADTOME-IV. Axial and in-plane resolutions of the PET images were each 4.5 mm (in full width at half maximum), and the slice thickness was 4 mm. Twenty minutes after MET injection (4 MBq/kg), an emission scan of the brain was performed for 10 min. The emission scan was reconstructed to a matrix of  $128 \times 128$  (using an iterative algorithm), and attenuation and scatter correction were done. The voxel size was  $2 \times 2 \times 3.25$  mm.

Ten patients were examined with Eminence-B. Axial and transaxial resolutions of the PET were each 4.5 mm (in full width at half maximum). The injection volume and timing of the scan were the same as HEADTOME-IV. The emission scan was reconstructed to a matrix of  $128 \times 128$ , and attenuation and scatter correction were done. The voxel size was  $2 \times 2 \times 3.25$  mm.

One patient was examined with Biograph-16. Axial and transaxial resolutions of the PET were 5.5 and 5.9 mm (in full width at half maximum), respectively. The injection volume and timing of the scan were the same as HEADTOME-IV. The emission scan was reconstructed to a matrix of  $336 \times 336$ , and attenuation and scatter correction were done. The voxel size was  $1.02 \times 1.02 \times 2$  mm.

All MET PET images were interpreted by an experienced neurosurgeon. The MET uptake was calculated by drawing a region of interest (ROI) using a freehand procedure. In all cases, MET uptake of the lesion was higher than in normal gray matter. In cases with a multiple meningioma, the lesion with the highest mass was evaluated. From the tumor lesion and normal reference region (frontal lobe of the normal side), the lesion to normal ratio (LN ratio) of mean MET uptake was calculated.

Surgical resection, pathological findings, and clinical follow-up

Thirty-three cases were treated with surgery, and four cases were observed. In surgical cases, GTR (Simpson grade I or II) was performed in 18 cases (55 %), and subtotal resection (Simpson grade III or IV) was performed in 13 cases (39 %). Partial resection (Simpson grade IV) was performed in one case (3 %), and a biopsy (Simpson grade V) was performed in one case (3 %). The pathological diagnosis and the WHO grade were determined by experienced

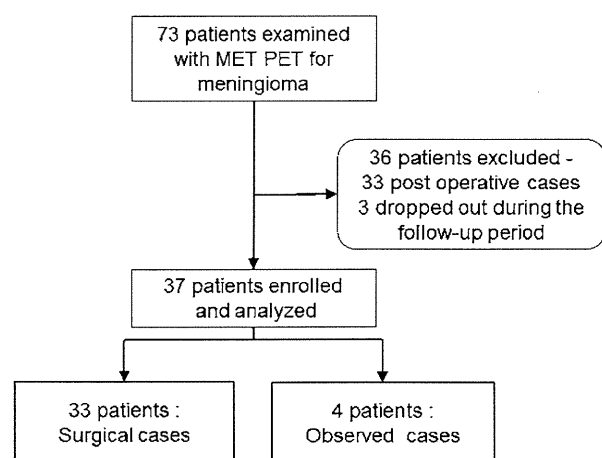


**Fig. 1** Analysis of meningioma cases with MET PET

pathologists according to the WHO classification updated in 2007. The Ki-67 LI was also calculated. All patients were followed up at our out-patient clinic without any additional treatment for the tumor during the follow-up period. For the surgical cases, gadolinium (Gd)-enhanced magnetic resonance imaging (MRI) was performed every 3–6 months in the first 2 years after surgery, and then every year during the follow-up period. For the observation cases, Gd-enhanced MRI was performed more than once a year. The mean follow-up period was  $80 \pm 52$  months (range 4–180 months). In surgical cases, the lesion was defined as a ‘recurrence’ when a lesion was found at the same location or a residual lesion was obviously enlarged in the radiological examinations. In non-surgical observation cases, the lesion was defined as a ‘progression’ when the tumor size was obviously enlarged in the radiological examinations.

We evaluated the risk factors for recurrence and progression by age, gender, location (skull base or not), extent of resection (GTR or not), Ki-67 LI, and LN ratio of MET uptake.

#### Statistical analysis

We evaluated the risk factors for recurrence and progression using paired *t* tests. When the data were not normally distributed, Wilcoxon’s rank-sum test was used for continuous data. Fisher’s exact tests were used for categorical data. Cox proportional hazards regression analysis was used for the surgical cases to assess the predictors of recurrence and progression with duration of the recurrence-free period as the time variable. A receiver operating characteristics (ROC) curve was assessed to confirm the best cutoff value of the LN ratio for recurrence and progression. All statistical analysis was performed using JMP 9 software (SAS Institute Inc.).

## Results

#### Characteristics and pathology

During the follow-up period, six surgical patients had a recurrence, and two observation patients progressed. The characteristics of the 37 cases are shown in Table 1. Summaries of the recurrence group and the non-recurrence group are shown in Table 2. The mean age of the recurrence group was  $57.9 \pm 11.8$  years, and that of the non-recurrence group was  $53.6 \pm 13.2$  years. We found no significant difference in the numbers of males and females in each group.

The tumor location is shown in Table 1. We classified the tumor location into two groups: skull base and non-skull base. The recurrence rate was not significantly different between these two groups.

Two patients died during the clinical follow-up period. One (case 20) died of thyroid cancer 51 months after PET examination, and another (case 21) died due to tumor progression 4 months after PET examination. The tumors were classified by pathology as follows. Ten were meningothelial (30 %), nine were fibrous (27 %), eight were transitional (24 %), two were angiomatous (6 %), two were chordoid (6 %), one was secretory (3 %), and one was atypical (3 %). Thirty cases were WHO grade I meningiomas, and three cases were WHO grade II meningiomas. The recurrence rate was not significantly different between WHO grade I (17 %, 5/30 cases) and grade II (33 %, 1/3 cases). The mean LN ratio of WHO grade I meningiomas was  $2.99 \pm 1.07$ , and the mean LN ratio of WHO grade II meningiomas was  $2.35 \pm 0.36$ . The LN ratio was not significantly different between WHO grade I and grade II.

#### Extent of tumor resection and recurrence

Gross total resection was performed in 18 patients, and one patient (case 35) had a recurrence during clinical follow-up. In 15 patients, some tumor remained after the surgery. In this non-GTR group, recurrence of meningioma was observed in five patients. The recurrence rate was not significantly different between the non-GTR group and the GTR group ( $p = 0.053$ ).

#### LN ratio of MET PET and Ki-67 LI for progression and recurrence

During the clinical follow-up, six cases of recurrence and two cases of progression were found. The average LN ratio of these eight cases was  $3.67 \pm 1.15$  [95 % confidence interval (CI) 2.71–4.64] and that of the remaining 29 cases was  $2.65 \pm 0.86$  (95 % CI 2.32–2.98). The average LN ratio of the cases with recurrence and progression was higher than that of the cases without recurrence or progression ( $p < 0.01$ , Fig. 2). The average Ki-67 LI of the recurrent six cases was  $1.81 \pm 1.21$  (95 % CI 0.54–3.09), and that of the 27 cases without recurrence was  $3.06 \pm 3.84$  (95 % CI 1.54–4.58). The Ki-67 LI was not significantly different between the recurrence group and the non-recurrence group ( $p = 0.44$ ). No correlation was found between the LN ratio and the Ki-67 LI (Fig. 3). Risk factors evaluated with univariate analysis are summarized in Table 2. One illustrative case is shown in Fig. 4.

**Table 1** Characteristics of 37 patients with meningioma

No.	Age (years)	Gender	Location	Pathological diagnosis	WHO grade	Ki-67	LN ratio	Surgery	Recurrence/ progression (months after pet exam)	Follow-up (months)
1	48	F	Parasagittal	Transitional	I	15.5	2.23	GTR	No	176
2	67	F	Parasagittal	Transitional	I	3	2.22	GTR	No	45
3	49	F	Sphenoid ridge	Chordoid	II	1.34	2.63	GTR	No	157
4	57	F	Petroclival	Secretory	I	14.4	3.00	GTR	No	40
5	49	M	Olfactory groove	Transitional	I	4.98	2.63	GTR	No	180
6	39	M	Pineal	Chordoid	II	3.03	1.95	GTR	No	26
7	61	F	Clival	Fibrous	I	4	5.10	STR	Yes (9)	141
8	43	M	Parasagittal	Fibrous	I	0.3	3.97	GTR	No	159
9	58	F	Parasagittal	Fibrous	I	1.45	3.10	GTR	No	34
10	46	F	Convexity	Fibrous	I	4.49	3.73	GTR	No	88
11	61	M	Clinoidal	Transitional	I	1.12	2.94	STR	No	152
12	79	M	Convexity	Meningothelial	I	1.26	5.38	STR	Yes (13)	56
13	57	F	Parasagittal	Angiomatous	I	2.29	3.61	STR	Yes (20)	147
14	37	F	Convexity	Meningothelial	I	2.27	3.37	GTR	No	145
15	54	F	Tentorial	Fibrous	I	0.59	3.32	STR	No	142
16	71	M	Parasagittal	Meningothelial	I	0.92	5.09	STR	No	65
17	66	F	C-P angle	Transitional	I	0.49	2.65	STR	No	138
18	22	F	Convexity	Meningothelial	I	1.3	1.98	GTR	No	130
19	60	M	Sphenoid ridge	Fibrous	I	1.33	2.90	STR	Yes (17)	71
20	74	M	Tuberculum sellae	Meningothelial	I	0.2	2.17	STR	No	51
21	39	M	Middle fossa	–	–	–	3.18	–	Yes (4)	4
22	75	F	C-P angle	Fibrous	I	3.5	2.35	GTR	No	54
23	52	F	Tuberculum sellae	Angiomatous	I	1	2.54	GTR	No	110
24	50	F	Sphenoid ridge	Meningothelial	I	1.26	1.65	STR	No	29
25	49	F	C-P angle	–	–	–	1.53	–	No	97
26	62	M	Convexity	Fibrous	I	3	2.86	STR	No	65
27	57	M	Convexity	Transitional	I	2.95	1.20	GTR	No	48
28	44	F	Foramen magnum	Meningothelial	I	5.6	2.64	GTR	No	48
29	48	F	Intraventricular	Fibrous	I	6.5	3.03	GTR	No	74
30	42	F	Sphenoid ridge	Transitional	I	2	2.73	STR	No	69
31	62	F	Convexity	Transitional	I	0.1	1.68	Biopsy	No	47
32	30	F	Intraventricular	–	–	–	2.49	–	No	24
33	69	F	Convexity	Meningothelial	I	0.3	1.27	GTR	No	43
34	49	M	Clivotentorial	–	–	–	2.39	–	Yes (43)	43
35	53	F	Intraventricular	Atypical	II	1.5	2.48	GTR	Yes (26)	26
36	65	M	Clival	Meningothelial	I	0.5	4.35	Partial	Yes (15)	25
37	72	M	Tentorial	Meningothelial	I	1	3.89	STR	No	23

C-P angle cerebello-pontine angle, GTR gross total resection, STR subtotal resection

In our study, the LN ratio was a significant risk factor for recurrence and progression with univariate analysis. We also evaluated risk factors using multivariate analysis. The results are summarized in Table 3. Multivariate analysis showed that the LN ratio, the extent of resection, and the WHO grade were significant risk factors for recurrence and progression. The hazard ratio of the LN

ratio was 4.21. The LN ratio was the only factor examined preoperatively.

ROC curve analysis

A ROC curve was generated, and the area under the curve (AUC) was calculated to determine the best discriminating

**Table 2** Evaluation of risk for recurrence and progression using univariate analysis

	Total cases		Recurrence/progression	Non-recurrence/progression	<i>p</i> value
Cases	37		8	29	
Age (years)	37		57.9 ± 11.8	53.6 ± 13.2	0.41
Gender	37	Female	3	20	0.22
		Male	5	9	
Skull base	37	Yes	5	11	0.25
		No	3	18	
LN ratio	37		3.67 ± 1.15	2.65 ± 0.86	<0.01
Extent of resection	33	GTR	1	17	0.053
		Non-GTR	5	10	
WHO grade	33	Grade I	5	25	0.46
		Grade II	1	2	
Ki-67 LI	33		1.81 ± 1.21	3.06 ± 3.84	0.44

The LN ratio was a significant risk factor for recurrence and progression

LN lesion to normal, GTR gross total resection, LI labeling index

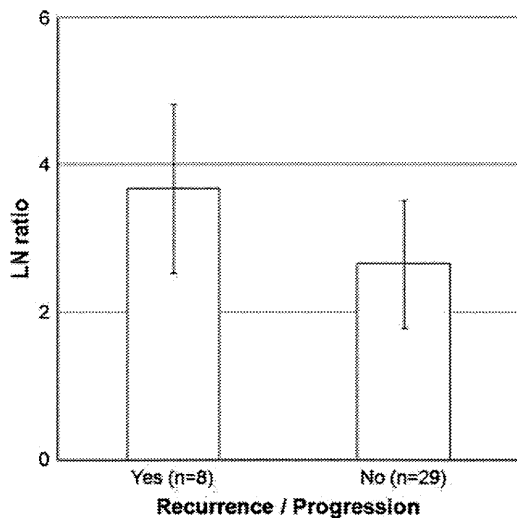


**Fig. 2** LN ratio of MET PET and recurrence/progression. The LN ratio in cases with recurrence and progression was significantly higher than that in cases without recurrence and progression ( $p < 0.01$ )

level of the LN ratio for predicting recurrence and progression. ROC analysis confirmed 3.18 as the best predictive cutoff value of the LN ratio for recurrence and progression. The AUC was 0.754. Using the best cutoff value of 3.18, the sensitivity and specificity were 63 and 79 %, respectively (Fig. 5).

## Discussion

The risk factors for recurrence and progression in meningioma have been reported in many previous studies. They include age [5, 6], gender [7], tumor size [8], calcification [7,

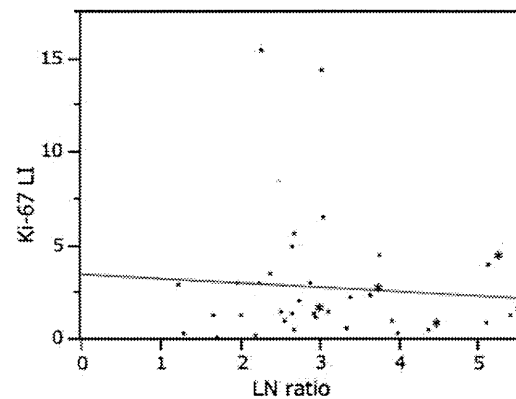


**Fig. 3** Correlation between the LN ratio of MET PET and the Ki-67 LI. No correlation between the LN ratio and the Ki-67 LI was observed. Asterisks cases with recurrence or progression

9], brain invasion [10], location [11], vascular density [12], Ki-67 LI [8, 13–15], extent of the resection [12, 16, 17], and WHO grade [11]. In our study, age, gender, tumor location, Ki-67 LI, and the LN ratio of MET PET were investigated. A high LN ratio was significantly correlated with tumor recurrence and progression. However, age, gender, tumor location, and Ki-67 LI were not significantly correlated with tumor recurrence. These risk factors remain controversial.

Recently, the MET PET method has been used in gliomas and other intracranial tumors to evaluate the malignancy of the tumor and the proliferative activity. In previous studies of gliomas, MET uptake correlated with the WHO grade, Ki-67 LI, and patient survival [18–21]. However, the role of MET PET in meningioma is not clear. In a previous study using  $^{18}\text{F}$ -fluorodeoxyglucose (FDG) PET,  $^{18}\text{F}$ -FDG uptake was correlated with the Ki-67 LI but not with recurrence of the meningioma [22, 23]. Using

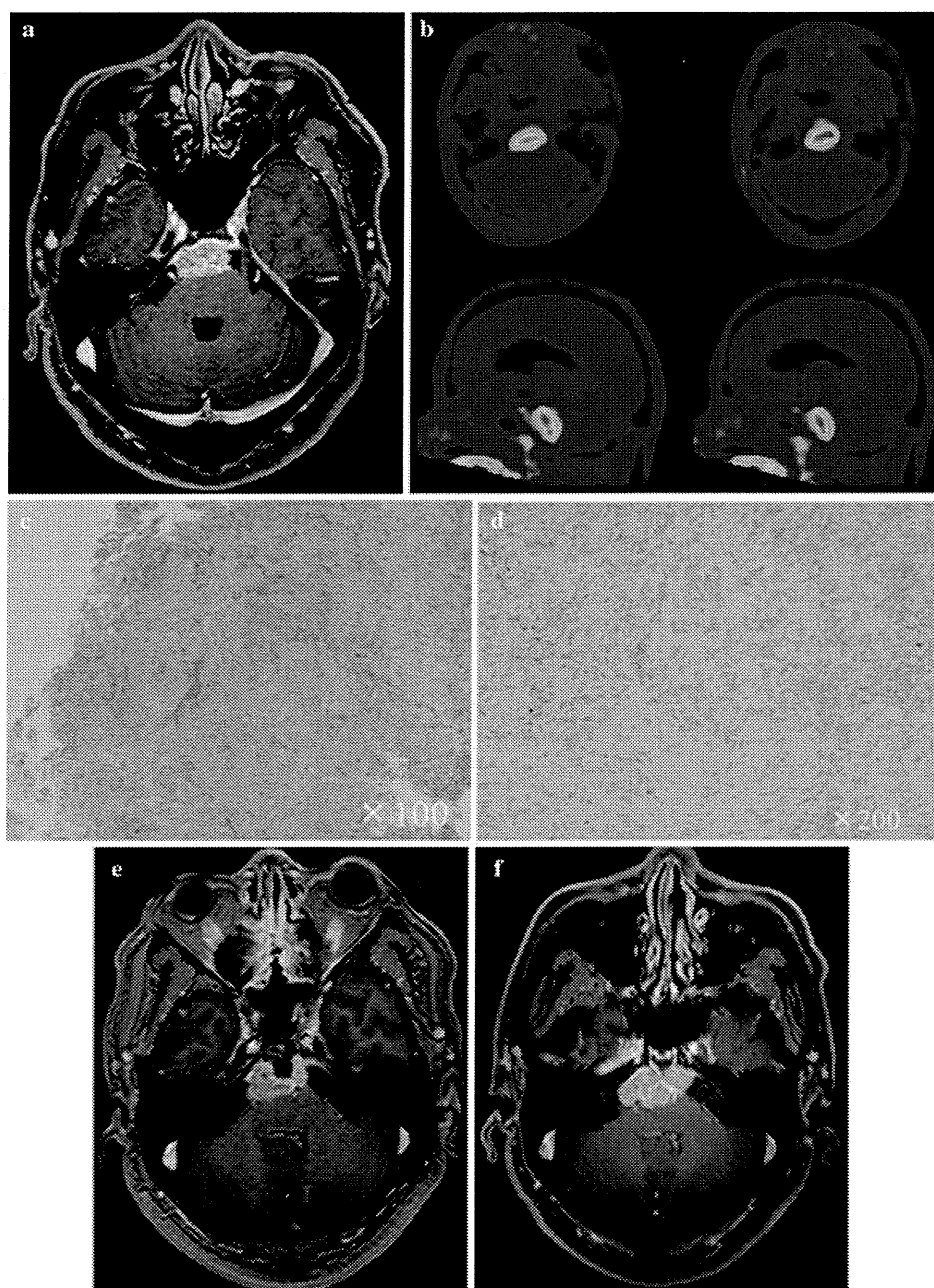


**Fig. 4** Case 36. **a** Preoperative Gadolinium (Gd)-enhanced T1-weighted image. The tumor is located at the clivus. **b**  $^{11}\text{C}$ -methionine was taken up into the tumor. The LN ratio was 4.35. **c**, **d** Photomicrograph of a sample of the lesion. Hematoxylin and eosin-stained section (**c**  $\times 100$ ) and Ki-67 staining (**d**  $\times 200$ ) of a meningioma tissue

specimen. The diagnosis based on pathology was meningeothelial meningioma. The Ki-67 LI was 0.5. **e** Postoperative Gd-enhanced T1-weighted image. In this case, the tumor was partially removed using a trans-sphenoidal approach. **f** Gd-enhanced T1-weighted image 15 months after surgery. The tumor had begun to grow again

kinetic analysis with  $^{18}\text{F}$ -FDG PET, Tsuyuguchi [24] showed that the kinetic rate constant of glucose metabolism is related to the Ki-67 LI. However, that analysis requires frequent arterial blood samplings and dynamic PET scanning. The procedure is very complicated and not practical for clinical use. Moreover, the results of  $^{18}\text{F}$ -FDG PET are

influenced by blood glucose. In patients with hyperglycemia, the results may lead to overestimation [25]. Iuchi et al. [26] showed that MET uptake is significantly correlated with the count of nuclear organizer regions, which is a histological index of protein synthesis, the Ki-67 LI, and a histological index of proliferative activity. In that study,

$^{18}\text{F}$ -FDG uptake showed no significant correlation with the Ki-67 LI or clinical malignancy. The uptake of methionine reflects amino acid transport and metabolism, but this does not mean that methionine uptake is correlated with protein

**Table 3** Evaluation of risk factors for recurrence using Cox proportional hazards model

	<i>p</i> value	Risk ratio
Age (years)	0.28	
Gender	0.43	
Skull base	0.12	
LN ratio	0.03	4.21
Extent of resection (non-GTR/GTR)	0.014	
WHO grade (grade II/grade I)	0.0074	
Ki-67 LI	0.079	

LN ratio, extent of resection, and WHO grade were significant risk factors

LN lesion to normal, WHO World Health Organization, GTR gross total resection, LI labeling index

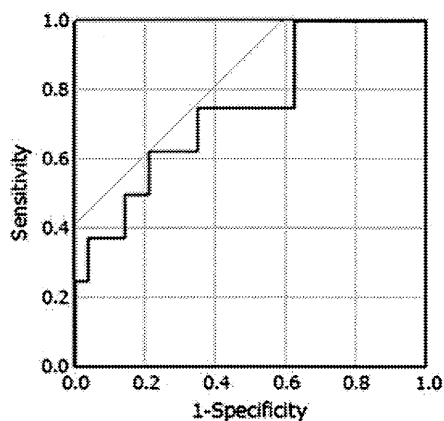


**Fig. 5** ROC curve of the LN ratio. AUC of the LN ratio of MET PET was 0.754. The optimal cutoff value was 3.18. The sensitivity and specificity were 63 and 79 %, respectively

**Table 4** Evaluation of risk factors for recurrence and progression excluding gross total resection cases

	Total cases	Recurrence/progression	Non-recurrence/progression	<i>p</i> value	
Cases	19	7	12		
Age (years)	19	58.6 ± 12.5	57.8 ± 13.2	0.9	
Gender	19	Female	2	7	0.35
		Male	5	5	
Skull base	19	Yes	5	6	0.63
		No	2	6	
LN ratio	19	3.84 ± 1.13	2.74 ± 1.02	0.04	
Surgical cases		5	10		
WHO grade	15	Grade I	5	10	0.18
		Grade II	0	0	
Ki-67 LI	15	1.87 ± 1.35	1.06 ± 0.87		

Only the LN ratio was significantly different between the recurrence/progression group and the non-recurrence/progression group

LN lesion to normal, WHO World Health Organization, LI labeling index

synthesis and proliferation [27]. Some previous studies have shown that MET uptake correlates with microvessel density in glioma cases [28, 29], but in meningioma cases, MET uptake does not correlate with microvessel density [30]. This observation may reflect the fact that meningioma has multiple pathological subtypes and, thus, microvessel density may be different in each subtype. To evaluate the correlation between the LN ratio and microvessel density in meningioma, many cases of each subtype would be necessary.

Arita et al. [30] showed that the LN ratio of MET uptake is not significantly correlated with tumor doubling time. In this study, many asymptomatic patients were enrolled, and the mean tumor doubling time was very long ( $174 \pm 270$  months) despite a short follow-up period ( $26.7 \pm 16.7$  months). Thus, evaluation of recurrence and progression in meningioma using tumor doubling time appeared to be difficult because most meningiomas progress slowly.

Compared with  $^{18}\text{F}$ -FDG PET, the contrast between a meningioma lesion and normal brain tissue is clear in MET PET and, thus, we can correctly define the ROI using MET PET. Recently, we have evaluated MET uptake more correctly by fusing PET images with computed tomography or MR images.

In this study, we calculated the LN ratio using the mean MET uptake of the lesion and the normal brain tissue. The methionine uptake in the tumor depends not only on the metabolic rate, but also on the vascular bed [31]. The vascular bed of the meningioma is different within the various pathological types of meningiomas [32], and the vascular bed may be variable in the same specimen. Biological activity is heterogeneous in the same meningioma lesion [33, 34]. Thus, partially high MET uptake does not always indicate a high metabolic rate of the whole tumor. In this study, we used the mean MET uptake, not the maximum MET uptake, to reduce the influence on the heterogeneity of MET uptake.

In this study, tumor progression and recurrence were not significantly different between the GTR and non-GTR groups. However, in some cases with a high Ki-67 LI, GTR was performed, and the recurrence rate was low. GTR was a factor that strongly influenced the recurrence rate. We evaluated the recurrence and progression in the non-GTR group. The LN ratio in the group with recurrence and progression was also significantly higher than that in the group without recurrence and progression ( $p < 0.05$ ). The Ki-67 LI was not significantly different ( $p = 0.18$ ). Our observations are summarized in Table 4.

In our study, the LN ratio was a significant risk factor for recurrence and progression. The LN ratio of MET PET may indicate the proliferative activity of meningioma. Using ROC analysis, the AUC was 0.754, and the best cutoff value was 3.18, resulting in a sensitivity and specificity of 63 and 79 %, respectively. The sensitivity and specificity of the LN ratio were not less than those of the Ki-67 LI, as described in a previous study [35, 36].

In our study, the Ki-67 LI was not significantly different between the patients with recurrence and those without. We also found no correlation between the LN ratio and the Ki-67 LI. Some previous papers have reported that the correlation between the Ki-67 LI and tumor recurrence is controversial [4, 33, 37, 38]. Meningioma is characterized by heterogeneous biological activity within the same tumor tissue [33, 34]. It is doubtful that the Ki-67 LI obtained from a small tumor specimen can adequately evaluate the proliferative potential of the whole tumor. In fact, MET uptake is heterogeneous in a large tumor and may reflect the heterogeneity of the Ki-67 LI. The MET PET method is useful for evaluating the whole tumor. The Ki-67 LI overlaps within each grade of meningioma [39–41]. Evaluating the proliferative activity of the whole tumor and providing an accurate prognosis may be difficult with only one index.

The extent of resection was a significant risk factor as shown in a previous study [12, 16, 17]. However, the location of the tumor was not a significant risk factor in this study. Sixteen cases of skull base meningioma were included. In these cases, total resection without complications is difficult. A GTR of the tumor would reduce the risk of recurrence. This result may indicate that additional treatments are necessary for a residual tumor in which the LN ratio is higher than 3.18.

The WHO grade of meningioma was also a significant risk factor. In this study, we investigated preoperative cases and, thus, most cases were WHO grade I; only three cases were WHO grade II. Cases with WHO grade III meningioma are relatively infrequent at initial diagnosis. Almost all cases of meningioma are pathologically benign. Thus, we have to follow patients for a long time to investigate malignant changes and the prognosis. We must investigate

additional consecutive cases to evaluate the largest number and the widest variety of cases.

Our study showed that the MET PET method has useful sensitivity and specificity for evaluation of recurrence and progression in meningioma. The most beneficial point is that  $^{11}\text{C}$ -methionine PET is not invasive, whereas analysis of the Ki-67 LI requires surgery. Thus, without surgery, we can evaluate the risk of progression and recurrence and consider the treatment strategy. We can determine the risk of progression and recurrence before deciding on observation or surgery. In asymptomatic cases, high LN ratio of MET PET may be the decisive factor for determining surgical treatment. We did not evaluate a large number of cases, and thus continued collection of cases and evaluation of the data are necessary.

## Conclusion

The results of our study showed that MET uptake by the meningioma was a significant prognostic factor. MET uptake was significantly higher in cases with recurrence or progression. The AUC of the LN ratio for recurrence or progression was 0.754, and the best cutoff value was 3.18. The greatest advantage associated with the MET PET method is its non-invasive nature.

**Acknowledgments** The authors appreciate the technical support of the radiological technologist at our institute.

**Conflict of interest** The authors have no personal financial or institutional interest in any of the drugs, materials, or devices described in this article.

## References

1. Committee of Brain Tumor Registry of Japan. Report of Brain Tumor Registry of Japan (1984–2000) *Neurol Med Chir.* 2009;49 Suppl.
2. Crompton MR, Gautier-Smith PC. The prediction of recurrence in meningiomas. *J Neurol Neurosurg Psychiatry.* 1970;33(1):80–7.
3. Jellinger K, Slowik F. Histological subtypes and prognostic problems in meningiomas. *J Neurol.* 1975;208(4):279–98.
4. Roser F, Samii M, Ostertag H, Bellinzona M. The Ki-67 proliferation antigen in meningiomas. Experience in 600 cases. *Acta Neurochir.* 2004;146(1):37–44 (discussion).
5. McCarthy BJ, Davis FG, Freels S, Surawicz TS, Damek DM, Grutsch J, et al. Factors associated with survival in patients with meningioma. *J Neurosurg.* 1998;88(5):831–9.
6. Nakamura M, Roser F, Michel J, Jacobs C, Samii M. The natural history of incidental meningiomas. *Neurosurgery.* 2003;53(1):62–70 (discussion-1).
7. Niuro M, Yatsushiro K, Nakamura K, Kawahara Y, Kuratsu J. Natural history of elderly patients with asymptomatic meningiomas. *J Neurol Neurosurg Psychiatry.* 2000;68(1):25–8.

8. Kasuya H, Kubo O, Tanaka M, Amano K, Kato K, Hori T. Clinical and radiological features related to the growth potential of meningioma. *Neurosurg Rev.* 2006;29(4):293–6 discussion 296–297.
9. Kuratsu J, Kochi M, Ushio Y. Incidence and clinical features of asymptomatic meningiomas. *J Neurosurg.* 2000;92(5):766–70.
10. Alvernia JE, Dang ND, Sindou MP. Convexity meningiomas: study of recurrence factors with special emphasis on the cleavage plane in a series of 100 consecutive patients. *J Neurosurg.* 2011;115(3):491–8.
11. McGovern SL, Aldape KD, Munsell MF, Mahajan A, DeMonte F, Woo SY. A comparison of World Health Organization tumor grades at recurrence in patients with non-skull base and skull base meningiomas. *J Neurosurg.* 2010;112(5):925–33.
12. Guevara P, Escobar-Arriaga E, Saavedra-Perez D, Martinez-Rumayor A, Flores-Estrada D, Rembao D, et al. Angiogenesis and expression of estrogen and progesterone receptors as predictive factors for recurrence of meningioma. *J Neurooncol.* 2010;98(3):379–84.
13. Matsuno A, Fujimaki T, Sasaki T, Nagashima T, Ide T, Asai A, et al. Clinical and histopathological analysis of proliferative potentials of recurrent and non-recurrent meningiomas. *Acta Neuropathol.* 1996;91(5):504–10.
14. Takeuchi H, Kubota T, Kabuto M, Kitai R, Nozaki J, Yamashita J. Prediction of recurrence in histologically benign meningiomas: proliferating cell nuclear antigen and Ki-67 immunohistochemical study. *Surg Neurol.* 1997;48(5):501–6.
15. Lanzafame S, Torrisi A, Barbagallo G, Emanuele C, Alberio N, Albanese V. Correlation between histological grade, MIB-1, p53, and recurrence in 69 completely resected primary intracranial meningiomas with a 6 year mean follow-up. *Pathol Res Pract.* 2000;196(7):483–8.
16. Adegbite AB, Khan MI, Paine KW, Tan LK. The recurrence of intracranial meningiomas after surgical treatment. *J Neurosurg.* 1983;58(1):51–6.
17. Mirimanoff RO, Dosoretz DE, Linggood RM, Ojemann RG, Martuza RL. Meningioma: analysis of recurrence and progression following neurosurgical resection. *J Neurosurg.* 1985;62(1):13–24.
18. Ribom D, Eriksson A, Hartman M, Engler H, Nilsson A, Langstrom B, et al. Positron emission tomography (11)C-methionine and survival in patients with low-grade gliomas. *Cancer.* 2001;92(6):1541–9.
19. Torii K, Tsuyuguchi N, Kawabe J, Sunada I, Hara M, Shiomi S. Correlation of amino-acid uptake using methionine PET and histological classifications in various gliomas. *Ann Nucl Med.* 2005;19(8):677–83.
20. Kim S, Chung JK, Im SH, Jeong JM, Lee DS, Kim DG, et al. 11C-methionine PET as a prognostic marker in patients with glioma: comparison with 18F-FDG PET. *Eur J Nucl Med Mol Imaging.* 2005;32(1):52–9.
21. Kato T, Shinoda J, Oka N, Miwa K, Nakayama N, Yano H, et al. Analysis of 11C-methionine uptake in low-grade gliomas and correlation with proliferative activity. *AJNR Am J Neuroradiol.* 2008;29(10):1867–71.
22. Lee JW, Kang KW, Park SH, Lee SM, Paeng JC, Chung JK, et al. 18F-FDG PET in the assessment of tumor grade and prediction of tumor recurrence in intracranial meningioma. *Eur J Nucl Med Mol Imaging.* 2009;36(10):1574–82.
23. Lippitz B, Cremerius U, Mayfrank L, Bertalanffy H, Raoofi R, Weis J, et al. PET-study of intracranial meningiomas: correlation with histopathology, cellularity and proliferation rate. *Acta Neurochirurgica Suppl.* 1996;65:108–11.
24. Tsuyuguchi N. Kinetic analysis of glucose metabolism by FDG-PET versus proliferation index of Ki-67 in meningiomas—comparison with gliomas. *Osaka City Med J.* 1997;43(2):209–23.
25. Cremerius U, Bares R, Weis J, Sabri O, Mull M, Schroder JM, et al. Fasting improves discrimination of grade 1 and atypical or malignant meningioma in FDG-PET. *J Nucl Med.* 1997;38(1):26–30.
26. Iuchi T, Iwadate Y, Namba H, Osato K, Saeki N, Yamaura A, et al. Glucose and methionine uptake and proliferative activity in meningiomas. *Neurol Res.* 1999;21(7):640–4.
27. Gudjonsson O, Blomquist E, Lilja A, Ericson H, Bergstrom M, Nyberg G. Evaluation of the effect of high-energy proton irradiation treatment on meningiomas by means of 11C-L-methionine PET. *Eur J Nucl Med.* 2000;27(12):1793–9.
28. Okubo S, Zhen HN, Kawai N, Nishiyama Y, Haba R, Tamiya T. Correlation of L-methyl-11C-methionine (MET) uptake with L-type amino acid transporter 1 in human gliomas. *J Neurooncol.* 2010;99(2):217–25.
29. Kracht LW, Friese M, Herholz K, Schroeder R, Bauer B, Jacobs A, et al. Methyl-[11C]-L-methionine uptake as measured by positron emission tomography correlates to microvessel density in patients with glioma. *Eur J Nucl Med Mol Imaging.* 2003;30(6):868–73.
30. Arita H, Kinoshita M, Okita Y, Hirayama R, Watabe T, Ishohashi K, et al. Clinical characteristics of meningiomas assessed by <sup>11</sup>C-methionine and <sup>18</sup>F-fluorodeoxyglucose positron-emission tomography. *J Neurooncol.* 2012;107(2):379–86.
31. Abe Y, Matsuzawa T, Itoh M, Ishiwata K, Fujiwara T, Sato T, et al. Regional coupling of blood flow and methionine uptake in an experimental tumor assessed with autoradiography. *Eur J Nucl Med.* 1988;14(7–8):388–92.
32. Kimura H, Takeuchi H, Koshimoto Y, Arishima H, Uematsu H, Kawamura Y, et al. Perfusion imaging of meningioma by using continuous arterial spin-labeling: comparison with dynamic susceptibility-weighted contrast-enhanced MR images and histopathologic features. *AJNR Am J Neuroradiol.* 2006;27(1):85–93.
33. Siegers HP, Zuber P, Hamou MF, van Melle GD, de Tribolet N. The implications of the heterogeneous distribution of Ki-67 labelled cells in meningiomas. *Br J Neurosurg.* 1989;3(1):101–7.
34. Abramovich CM, Prayson RA. Histopathologic features and MIB-1 labeling indices in recurrent and nonrecurrent meningiomas. *Arch Pathol Lab Med.* 1999;123(9):793–800.
35. Bruna J, Brell M, Ferrer I, Gimenez-Bonafe P, Tortosa A. Ki-67 proliferative index predicts clinical outcome in patients with atypical or anaplastic meningioma. *Neuropathology.* 2007;27(2):114–20.
36. Kim YJ, Ketter R, Henn W, Zang KD, Stuedel WI, Feiden W. Histopathologic indicators of recurrence in meningiomas: correlation with clinical and genetic parameters. *Virchows Archiv.* 2006;449(5):529–38.
37. Moller ML, Braendstrup O. No prediction of recurrence of meningiomas by PCNA and Ki-67 immunohistochemistry. *J Neurooncol.* 1997;34(3):241–6.
38. Nakaguchi H, Fujimaki T, Matsuno A, Matsuura R, Asai A, Suzuki I, et al. Postoperative residual tumor growth of meningioma can be predicted by MIB-1 immunohistochemistry. *Cancer.* 1999;85(10):2249–54.
39. Abramovich CM, Prayson RA. MIB-1 labeling indices in benign, aggressive, and malignant meningiomas: a study of 90 tumors. *Hum Pathol.* 1998;29(12):1420–7.
40. Kolles H, Niedermayer I, Schmitt C, Henn W, Feld R, Stuedel WI, et al. Triple approach for diagnosis and grading of meningiomas: histology, morphometry of Ki-67/Feulgen stainings, and cytogenetics. *Acta Neurochir.* 1995;137(3–4):174–81.
41. Langford LA, Cooksley CS, DeMonte F. Comparison of MIB-1 (Ki-67) antigen and bromodeoxyuridine proliferation indices in meningiomas. *Hum Pathol.* 1996;27(4):350–4.

RESEARCH ARTICLE

# Standardized Uptake Value in High Uptake Area on Positron Emission Tomography with $^{18}\text{F}$ -FRP170 as a Hypoxic Cell Tracer Correlates with Intratumoral Oxygen Pressure in Glioblastoma

Takaaki Beppu,<sup>1</sup> Kazunori Terasaki,<sup>2</sup> Toshiaki Sasaki,<sup>2</sup> Shunrou Fujiwara,<sup>1</sup> Hideki Matsuura,<sup>1</sup> Kuniaki Ogasawara,<sup>1</sup> Koichiro Sera,<sup>2</sup> Noriyuki Yamada,<sup>3</sup> Noriyuki Uesugi,<sup>3</sup> Tamotsu Sugai,<sup>3</sup> Kohsuke Kudo,<sup>4</sup> Makoto Sasaki,<sup>4</sup> Shigeru Ehara,<sup>5</sup> Ren Iwata,<sup>6</sup> Yoshihiro Takai<sup>7</sup>

<sup>1</sup>Department of Neurosurgery, Iwate Medical University, Uchimaru 19-1, Morioka 020-8505, Japan

<sup>2</sup>Cyclotron Research Center, Iwate Medical University, Morioka, Japan

<sup>3</sup>Department of Clinical Pathology, Iwate Medical University, Morioka, Japan

<sup>4</sup>Institute for Biomedical Sciences, Iwate Medical University, Morioka, Japan

<sup>5</sup>Department of Radiology, Iwate Medical University, Morioka, Japan

<sup>6</sup>Cyclotron and Radioisotope Center (CYRIC), Tohoku University, Sendai, Japan

<sup>7</sup>Department of Radiology and Radiation Oncology, Hirosaki University Graduate School of Medicine, Hirosaki, Japan

## Abstract

**Purpose:** The aim of this study was to clarify the reliability of positron emission tomography (PET) using a new hypoxic cell tracer, 1-(2-[ $^{18}\text{F}$ ]fluoro-1-[hydroxymethyl]ethoxy)methyl-2-nitroimidazole ( $^{18}\text{F}$ -FRP170).

**Procedures:** Twelve patients with glioblastoma underwent  $^{18}\text{F}$ -FRP170 PET before tumor resection. Mean standardized uptake value (SUV) and normalized SUV were calculated at regions within a tumor showing high (high-uptake area) and relatively low (low-uptake area) accumulations of  $^{18}\text{F}$ -FRP170. In these areas, intratumoral oxygen pressure (tpO<sub>2</sub>) was measured using microelectrodes during tumor resection.

**Results:** Mean tpO<sub>2</sub> was significantly lower in the high-uptake area than in the low-uptake area. A significant negative correlation was evident between normalized SUV and tpO<sub>2</sub> in the high-uptake area.

**Conclusion:** The present findings suggest that high accumulation on  $^{18}\text{F}$ -FRP170 PET represents viable hypoxic tissues in glioblastoma.

**Key words:** F-FRP170, PET, Hypoxia, Glioblastoma, Oxygen pressure, HIF1- $\alpha$

**Abbreviation:** Cu-ATSM,  $^{64}\text{Cu}$ -diacetyl-bis(N4-methylthiosemicarbazone);  $^{18}\text{F}$ -FRP170, 1-(2-[ $^{18}\text{F}$ ]fluoro-1-[hydroxymethyl]ethoxy)methyl-2-nitroimidazole;  $^{18}\text{F}$ -FAZA, 1- $\alpha$ -D-(5-deoxy-5-[ $^{18}\text{F}$ ]fluoroarabinofuranosyl)-2-nitroimidazole;  $^{18}\text{F}$ -FMISO, [ $^{18}\text{F}$ ]fluoromisonidazole; Gd-T1WI, Gadolinium-enhanced T1-weighted imaging; HIF, Hypoxic-inducible factor; MRI, Magnetic resonance imaging; ROI, Region of interest; T2WI, T2-weighted imaging; PET, Positron emission tomography; VEGF, Vascular endothelial growth factor

## Introduction

Almost all malignant solid tumors include hypoxic cells due to both excessive consumption and insufficient supply of oxygen within the tumor. Intratumoral hypoxia induces various biological characteristics in tumors. For instance, hypoxia in tumor activates the hypoxia-responsive elements such as hypoxia-inducible factors (HIFs), leading to transcription of target genes including vascular endothelial growth factor (VEGF). VEGF induces angiogenesis, and is also closely related to the proliferation and invasion of tumor. Gene instability caused by hypoxia must affect the differentiation of tumor cells. Intratumoral hypoxic conditions are disadvantageous in term of the production of peroxide radicals, which induces DNA damage under irradiation. Cancer stem cells existing within hypoxic tumor tissue have also been considered to represent a likely cause of radioresistance [1–3]. In glioblastoma, hypoxic conditions play a key role in the development of tumor characteristics. Neuroimaging enabling minimally invasive, objective, and quantitative evaluation of hypoxic conditions in glioblastoma would offer many clinical benefits in terms of diagnosis, selection of treatment, and prediction of prognosis.

Positron emission tomography (PET) using hypoxic cell tracers offers an attractive method for detecting hypoxic cells because it is simple, low-invasive, repeatable, and not limited in applicability to superficial tumors [4]. So far, hypoxic cells in brain tumors have been detected using PET with hypoxic cell tracers such as [ $^{18}\text{F}$ ]fluoromisonidazole ( $^{18}\text{F}$ -FMISO) [5–7], 1- $\alpha$ -D-(5-deoxy-5- $^{18}\text{F}$ )-fluoroarabino furanosyl)-2-nitroimidazole ( $^{18}\text{F}$ -FAZA) [8], and  $^{64}\text{Cu}$ -diacetyl-bis(N4-methylthiosemicarbazone) (Cu-ATSM) [9, 10]. A new hypoxic cell tracer, 1-(2-[ $^{18}\text{F}$ ]fluoro-1-[hydroxymethyl]ethoxy)methyl-2-nitroimidazole ( $^{18}\text{F}$ -FRP170), has recently been identified [11, 12]. PET using  $^{18}\text{F}$ -FRP170 ( $^{18}\text{F}$ -FRP170 PET) has already been performed for detecting hypoxic cells in malignant brain tumors, and the potential of this new tracer has been documented [13]. Several studies assessing intratumoral oxygen condition using electrodes or other methods have confirmed reliability of PET with various hypoxic cell tracers other than  $^{18}\text{F}$ -FRP170 [14–17]. However, whether areas of high accumulation on  $^{18}\text{F}$ -FRP170 PET really represent tissues including hypoxic cells, and to what degree areas of high accumulation represent regions under hypoxic conditions have remained unclear. The aim of this study was to confirm the reliability of  $^{18}\text{F}$ -FRP170 PET for detecting hypoxic cells. We therefore compared standardized uptake value (SUV) measured on  $^{18}\text{F}$ -FRP170 PET with intratumoral oxygen pressure (tpO<sub>2</sub>) within glioblastoma measured using oxygen microelectrodes during tumor resection. Furthermore, we performed immunohistochemical detection HIF-1, a heterodimeric nuclear transcription factor playing a critical role in cellular response to low oxygen pressure [18], in tissues corresponding to the regions of interest (ROIs) on  $^{18}\text{F}$ -FRP170 PET images.

## Materials and Methods

### Patients

All study protocols were approved by the Ethics Committee of Iwate Medical University, Morioka, Japan (No. H22-70). Patients recruited to this study were admitted to Iwate Medical University Hospital between April 2008 and December 2012. Entry criteria for the study were: patients  $\geq 20$  years old with non-treated glioblastoma localized in cerebral white matter other than the brain stem or cerebellum, performance of  $^{18}\text{F}$ -FRP170 PET and measurement of absolute oxygen pressure within the tumor according to the study protocol, and voluntary provision of written informed consent to participate. Preoperative diagnosis was based on present history and findings from conventional magnetic resonance imaging (MRI) on admission, and final diagnosis of glioblastoma was made based on histological features after surgery. Twelve patients (ten men, two women, mean age,  $63 \pm 13.7$  years) were enrolled after excluding patients who did not meet the entry criteria (Table 1).

### $^{18}\text{F}$ -FRP170 PET

Within 7 days (mean,  $4.3 \pm 2.4$  days) before surgery for tumor resection, both conventional MRI including gadolinium-enhanced T1-weighted imaging (Gd-T1WI) and  $^{18}\text{F}$ -FRP170 PET were performed. The  $^{18}\text{F}$ -FRP170 was synthesized using on-column alkaline hydrolysis according to the methods described by Ishikawa et al. [12]. The final formulation for injection was formed in normal saline containing 2.5 %v/v ethanol using solid-phase extraction techniques. At 60 min after intravenous injection of approximately 370 MBq (mean,  $5.9 \pm 1.8$  MBq/kg) of  $^{18}\text{F}$ -FRP170, PET was performed using a PET/computed tomography (CT) system (SET3000 GCT/M; Shimazu, Japan). On  $^{18}\text{F}$ -FRP170 PET, ROIs of 10 mm in diameter were placed at areas of high accumulation (high-uptake area) and relatively low accumulation (low-uptake area) within the tumor bulk (Fig. 1a, b). These ROIs were placed at regions as close to the brain surface as possible to allow easy and safe insertion of microelectrodes for measuring oxygen pressure during surgery. A ROI was also placed in apparent normal cerebral white matter of the contralateral side. SUV for each ROI was automatically determined. Although both mean and maximal values of SUV in ROI were measured, we defined the mean value of SUV as “SUV” in this study. The normalized SUV, defined as SUV for each high- or low-uptake area divided by SUV for the apparent normal cerebral white matter of the contralateral hemisphere, was also calculated.

Immediately before surgery for each patient, we created a fusion image that combined a three-dimensional  $^{18}\text{F}$ -FRP170 PET image with Gd-T1WI using a surgical navigation system (Stealth Station TRIA plus; Medtronic, Minneapolis, MN) in the operation room. On the fusion image, both high- and low-uptake areas were identified stereotactically for each patient (Fig. 2a d).

### Measurement of Intratumoral Oxygen Pressure During Surgery

Measurement of tpO<sub>2</sub> was performed during surgery for aggressive tumor resection. The tpO<sub>2</sub> level was measured using disposable

**Table 1.** Patient characteristics and measurement data

No.	Sex	Age (year)	Location	SUV			Normalized SUV		tpO <sub>2</sub> (mmHg)		PaO <sub>2</sub> (mmHg)	HIF-1 $\alpha$ staining
				High uptake	Low uptake	ANWM	High uptake	Low uptake	High uptake	Low uptake		
1	M	76	Parietal lobe	0.99	0.54	0.54	1.83	1.00	23	44	157	-
2	M	81	Parietal lobe	2.22	1.39	1.04	2.13	1.34	16	45	128	-
3	M	59	Frontal lobe	1.46	1.16	0.87	1.69	1.33	28	56	176	-
4	F	61	Frontal lobe	1.10	0.87	0.74	1.49	1.18	32	54	145	-
5	M	75	Parietal lobe	1.83	1.11	0.83	2.20	1.34	16	33	143	-
6	F	54	Parietal lobe	1.43	0.82	0.62	2.31	1.32	30	54	134	-
7	M	64	Temporal lobe	1.62	1.00	0.72	2.25	1.39	15	27	158	+
8	M	54	Occipital lobe	1.50	1.01	0.76	1.97	1.33	17	35	120	+
9	M	67	Frontal lobe	1.84	1.46	1.13	1.63	1.29	25	36	132	+
10	M	76	Temporal lobe	1.90	0.92	0.77	2.47	1.19	15	26	124	+
11	M	58	Frontal lobe	1.37	1.25	0.90	1.52	1.39	24	34	137	+
12	M	31	Frontal lobe	1.66	1.11	0.87	1.91	1.28	20	37	148	+

ANWM apparent normal white matter, tpO<sub>2</sub> intratumoral oxygen pressure

Clark-type electrodes (UOE-04TS; Unique Medical, Tokyo, Japan) at the tip of a sensor (Teflon-coated tube; diameter, 0.4 mm; length, 10 mm). Immediately before surgery, electrodes were sterilized by immersion in a solution of 2.25 w/v% glutaraldehyde and buffer for 2 h, then washed with sterilized physiological saline solution. The electrode was then connected to a digital oxygen pressure monitor (POG-203; Unique Medical) to calibrate the value of oxygen pressure to 150 mmHg in a sterilized physiological saline solution prior to insertion into the tumor. After craniotomy, we stereotactically inserted a needle-shaped navigating marker of 2 mm in diameter into the center region of the high-uptake area where the ROI had been placed before surgery through the dura mater, while we observed the localization of the tip of the marker in the tumor on the monitor of the surgical navigation system (Fig. 2c, d). After removal of the navigation marker, we immediately inserted the electrode along the same trajectory through the dura mater, with the tip of the electrode placed within tumor tissue of the high-uptake area. A digital monitor was then used to measure tpO<sub>2</sub>. We observed tpO<sub>2</sub> value gradually declined from 150 mmHg while rising and falling on the digital monitor, and defined the minimum value as the absolute tpO<sub>2</sub> value at the high-uptake area for each patient. After completely washing and calibrating the value of oxygen pressure to 150 mmHg in a sterilized physiological saline solution, the same procedure described above was performed to measure tpO<sub>2</sub> in the low-uptake area. During measurements of tpO<sub>2</sub>, arterial oxygen pressure (PaO<sub>2</sub>) was measured using arterial blood obtained from the radial artery. After measuring tpO<sub>2</sub> and removing the electrode, we inserted a needle for biopsy along a trajectory to obtain tumor tissues from the high- and low-uptake areas in six patients. In all cases, the tumor was successfully removed after completing the procedures described above.

### HIF-1 $\alpha$ Immunohistochemistry

Immunohistochemical staining of HIF-1 $\alpha$  was performed on specimens obtained from tumor resection for six patients. From all specimens in both high- and low-uptake areas, paraffin-embedded tissue sections of 3- $\mu$ m-thickness were collected onto 3-aminopropyltriethoxylane-coated glass slides. The dewaxed preparations were given microwave pretreatment for 30 min in sodium citrate. The preparations were incubated for 60 min using

rabbit anti-HIF-1 $\alpha$  monoclonal antibody (clone, H1 $\alpha$ 67; Novus Biologicals, Littleton, CO) at 1:200 dilution. Preparations were incubated using peroxidase-based EnVision kits (Dako Japan, Tokyo, Japan) as the secondary antibody, then immersed in diaminobenzidine/H<sub>2</sub>O<sub>2</sub> solution for colored visualization. Finally, preparations were counterstained with hematoxylin.

We observed the staining attitude of HIF-1 $\alpha$  in tumor cells for all patients. We also evaluated the HIF-1 $\alpha$  staining indices for each high- or low-uptake area for each patient, defined as the percentage of cells showing nuclear staining as determined by counting approximately 1,000 cells under light microscopy ( $\times$ 400 magnification).

### Statistical Analyses

In all patients, differences in SUV, normalized SUV, and HIF-1 $\alpha$  staining index were compared between high- and low-uptake areas using the Mann Whitney *U* test. Differences in intratumoral pO<sub>2</sub> between high- and low-uptake areas were also compared in all patients using the Mann Whitney *U* test. Correlations between PaO<sub>2</sub> and tpO<sub>2</sub> and between normalized SUV and tpO<sub>2</sub> for all patients were analyzed in each high- and low-uptake area using Pearson's correlation coefficient test.

## Results

Scanning at 60 min after intravenous injection of tracer provided fine contrast images that enabled visual differentiation between high- and low-uptake areas in all patients. In eight patients with glioblastoma presenting a central necrotic region, <sup>18</sup>F-FRP170 was partially accumulated in the intermediate layer between the deep layer surrounding the central necrotic region and the outer layer within the peripheral region of tumor involved in lesion enhancement on Gd-T1WI (Fig. 1a, b). Fusion images combining Gd-T1WI and <sup>18</sup>F-FRP170 PET provided precise locations of both high- and low-uptake regions during surgery, and allowed us to successfully insert electrodes and obtain the

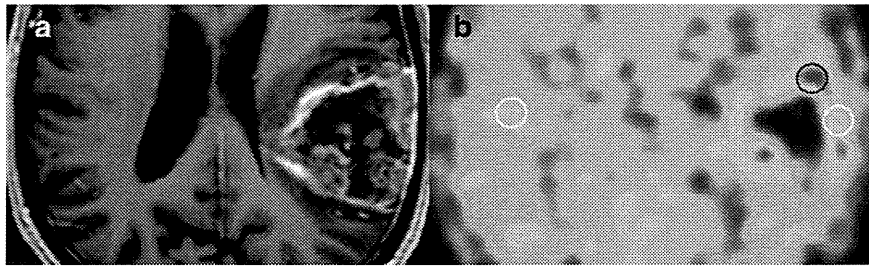


Fig. 1. Typical findings of  $^{18}\text{F}$ -FRP170 PET in glioblastoma with a large area of central necrosis in Case 1. High-uptake areas are seen partially in the area between the outer peripheral region showing enhancement on Gd-T1WI and a deeper region adjacent to the central necrotic region. ROIs were placed on a high-uptake area (*black circle*) and a relatively low-uptake area (*white circle*) within the tumor bulk showing enhancement on Gd-T1W, and also on apparent normal white matter of the contralateral hemisphere (*white circle*). a Gd-T1WI, b  $^{18}\text{F}$ -FRP170 PET.

sampling tissues (Fig. 2a-d). No patient presented with any complications due to  $^{18}\text{F}$ -FRP170 PET.

Mean SUV for high-uptake areas, low-uptake areas, and contralateral normal white matter regions were  $1.58 \pm 0.35$ ,  $1.05 \pm 0.25$ , and  $0.82 \pm 0.16$ , respectively. Significant differences in mean SUV were found between high- and low-uptake areas ( $p=0.001$ ), between high-uptake areas and normal white matter ( $p<0.001$ ), and between low-uptake

areas and normal white matter ( $p=0.01$ ), although SUV values in the three groups overlapped (Fig. 3a). Mean normalized SUV for the high- and low-uptake areas were calculated as  $1.95 \pm 0.33$  and  $1.28 \pm 0.11$ , respectively. Mean normalized SUV for the high-uptake area differed significantly ( $p<0.001$ ) and clearly from that of the low-uptake area, with a cut-off level of around 1.4 (Fig. 3b). Mean  $\text{tpO}_2$  was significantly lower in high-uptake areas ( $21.7 \pm$

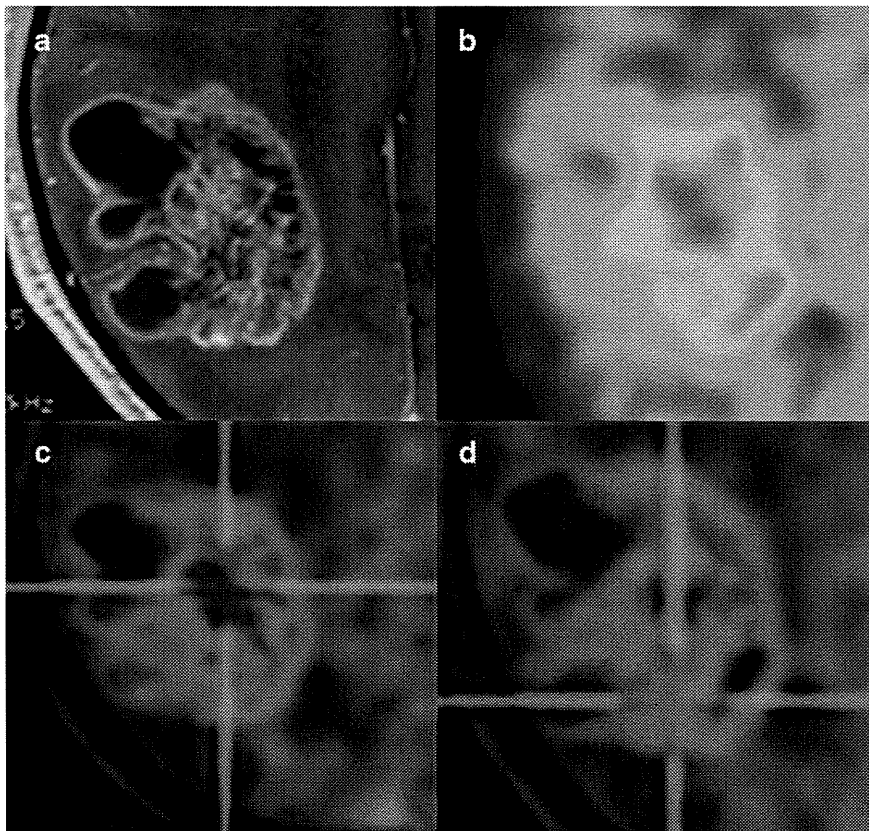
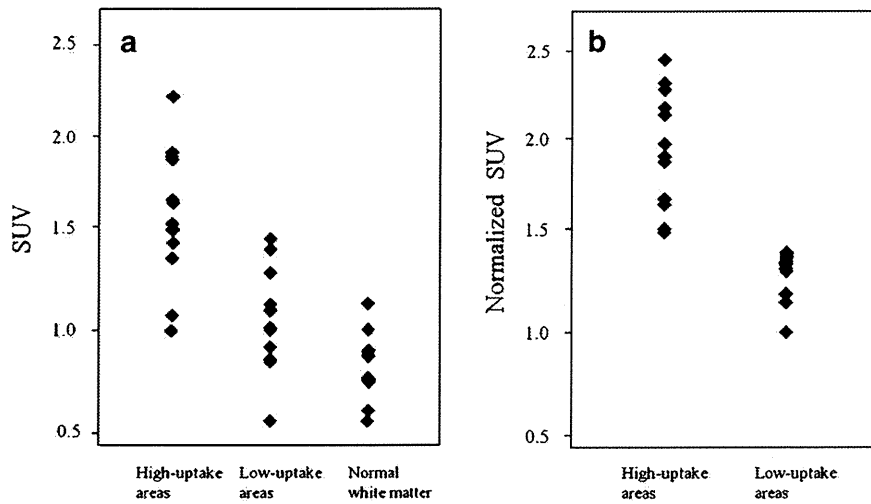


Fig. 2. High- and low-uptake areas were stereotactically localized on fusion images combining Gd-T1WI (a) and  $^{18}\text{F}$ -FRP170 PET (b) for Case 5, to identify tumor tissues corresponding to ROIs. On fusion images, high- and low-uptake areas were depicted as bluish regions (c) and greenish regions (d), respectively.



**Fig. 3.** **a** Differences in SUV among the high-uptake area, low-uptake area, and apparent normal white matter. **b** Difference in normalized SUV between high- and low-uptake areas.

6.2 mmHg) than in low-uptake areas ( $40.1 \pm 10.4$  mmHg;  $p < 0.001$ , Fig. 4). In terms of the relationship between normalized SUV and  $tpO_2$  in all patients, a significant negative correlation was found in high-uptake areas ( $r = -0.64$ ,  $p = 0.03$ ), whereas no significant correlation was identified in low-uptake

areas (Fig. 5a, b). No significant correlations between  $PaO_2$  and  $tpO_2$  were found in either high- or low-uptake areas (not shown).

On specimens obtained from high-uptake areas, HIF-1 $\alpha$  was clearly detectable in nuclei in all six patients, with three patients also showing HIF-1 $\alpha$  staining in cytoplasm. On the other hand,

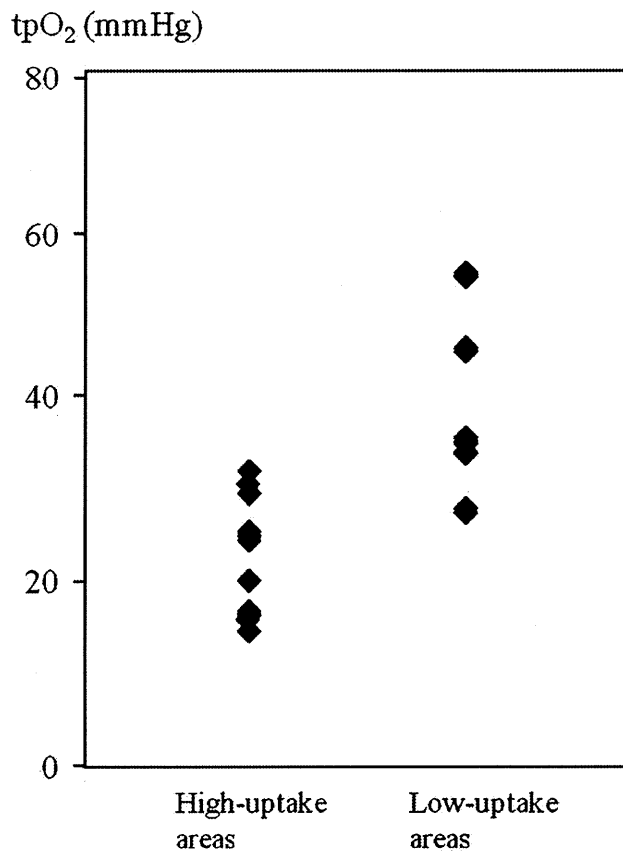


**Fig. 4.** Difference in  $tpO_2$  between high- and low-uptake areas.

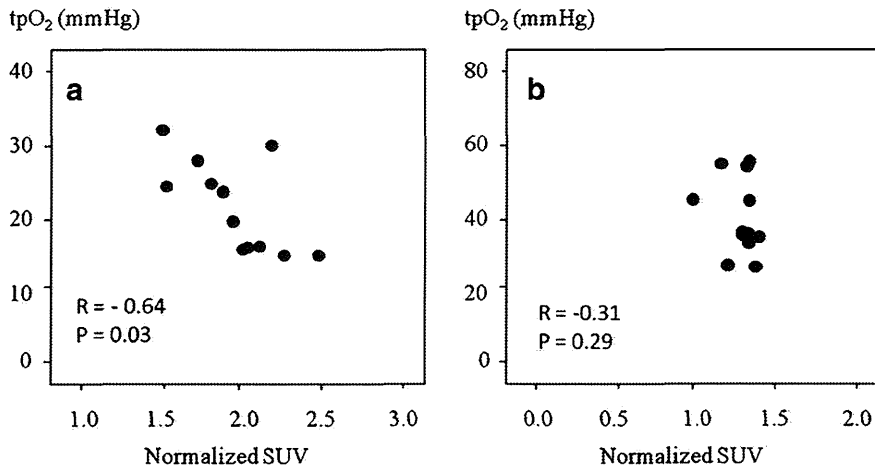


Fig. 5. Correlations between normalized SUV and tpO<sub>2</sub> in high-uptake areas (a) and low-uptake areas (b).

specimens from low-uptake areas showed three different patterns, with HIF-1α staining only cytoplasm in three patients, and both nuclei and cytoplasm in two patients. In the remaining patient, few barely surviving cells with HIF-1α staining were seen within a wide area of necrotic tissue (Fig. 6a–d). HIF-1α staining indices ranged from 35.2 to 63.5 % in high-uptake

areas, and from 8.9 to 35.9 % in low-uptake areas. Mean HIF-1α staining index was significantly higher in high-uptake areas (mean, 53.0±10.2 %) than in low-uptake areas (mean, 18.9±9.5 %). Notably, HIF-1α staining index was markedly low (8.9 %) in necrotic tissue obtained from a low-uptake area in one patient.

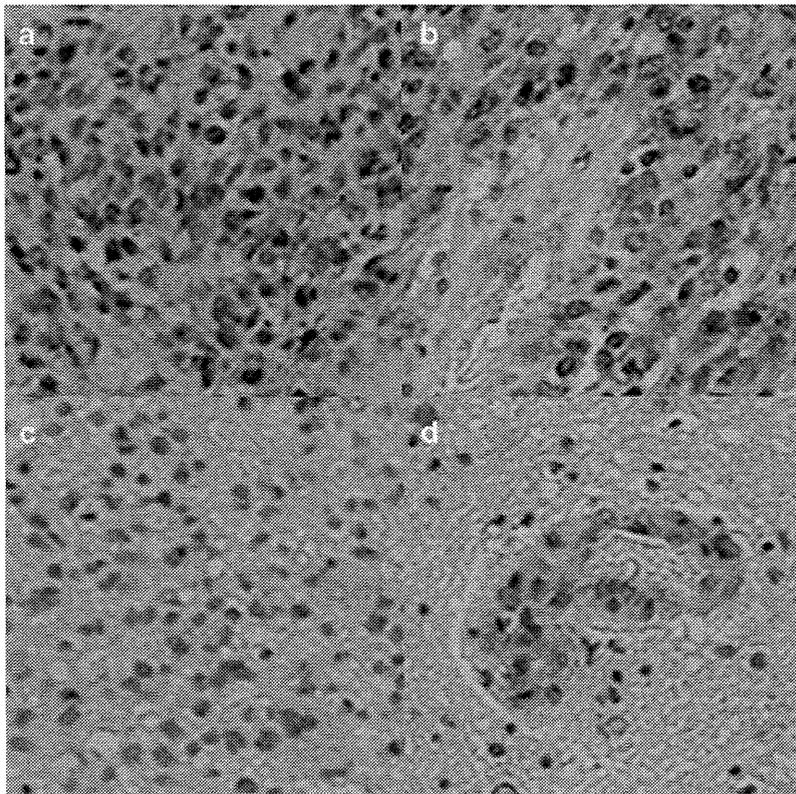


Fig. 6. Findings for HIF-1α immunostaining of tissues from high-uptake areas (a, b) and low-uptake areas (c, d). a HIF-1α was strongly detected in nuclei in all patients. b HIF-1α was stained in both cytoplasm and nuclei in three patients. c HIF-1α was stained only in cytoplasm in three patients. d A few HIF-1α-stained cells were seen within a wide necrotic tissue in one patient.

## Discussion

The present study showed that mean values of both SUV and normalized SUV were significantly higher in high-uptake areas than in low-uptake areas. In particular, normalized SUV values in high-uptake areas were absolutely higher than those in low-uptake areas. In this study, approximately 370 MBq of  $^{18}\text{F}$ -FRP170 was administered intravenously for all patients, according to a report by Shibahara et al. [13]. Absolute SUV might thus have been subtly influenced by the delivered volume of tracer into the tumor as determined by individual parameters, such as body size, cardiac output volume, and blood pressure. As normalization of absolute SUV can eliminate differences in these factors, we emphasize the importance of estimation using normalized SUV. In the present study,  $\text{tpO}_2$  did not correlate with  $\text{PaO}_2$  at all. Two previous reports examining both  $\text{tpO}_2$  in brain tumors and  $\text{PaO}_2$  could not find any relationship between these measured values, although correlations were not estimated statistically [19, 20]. Our results support those previous reports and indicate that  $\text{tpO}_2$  was not influenced by  $\text{PaO}_2$  during surgery. Values of  $\text{tpO}_2$  were significantly lower in high-uptake areas ( $21.7 \pm 6.2$  mmHg) than in low-uptake areas ( $40.1 \pm 10.4$  mmHg). Furthermore, a significant correlation was found between normalized SUV and  $\text{tpO}_2$  in high-uptake areas. These results indicate that high-uptake areas where  $^{18}\text{F}$ -FRP170 accumulates show relatively more hypoxic conditions than low-uptake areas, suggesting the reliability of findings from  $^{18}\text{F}$ -FRP170 PET.

Selective accumulation of  $^{18}\text{F}$ -FRP170 in hypoxic cells has been considered to proceed as follows. First, the nitroimidazole moiety in  $^{18}\text{F}$ -FRP170 is responsible for the initial accumulation in hypoxic cells. After passive diffusion inside the cells, enzymatic nitroreduction by nitroreductase results in nitroimidazole changing to radical anions. Under normoxic conditions, these radical anions are reoxidized and diffuse out of the cells, whereas products comprising radical anions covalently bound to intracellular macromolecules are trapped within cells under hypoxic conditions [13, 21–23]. As a result,  $^{18}\text{F}$ -FRP170 can accumulate only within viable and active hypoxic cells, but cannot accumulate within normoxic cells or even hypoxic cells with low metabolism such as apoptotic or necrotic cells. A previous report assessing accumulation of  $^{18}\text{F}$ -FRP170 in a rat model of ischemic myocardium using autoradiography documented that  $^{18}\text{F}$ -FRP170 was observed only within viable hypoxic myocardial cells [11]. As absolute SUV must correlate with the concentration of PET tracer within the tissue, SUV on  $^{18}\text{F}$ -FRP170 PET should increase with a higher density of viable hypoxic cells within the tissues of the ROI. We think that such high-uptake areas represent glioblastoma tissue comprising a high density of viable hypoxic cells. In contrast, tissues of low-uptake areas might represent low densities of viable hypoxic cells. In other words, a majority of cells in low-uptake areas could not accumulate  $^{18}\text{F}$ -

FRP170 because of the presence of either viable cells containing relatively higher  $\text{tpO}_2$  than high-uptake area or low metabolic-hypoxic cells degenerating in apoptosis or necrosis. The oxygen environment may thus differ substantially among different regions in low-uptake areas, despite the similar content of viable hypoxic cells. Indeed,  $\text{tpO}_2$  levels showed a wide range in low-uptake areas, with a large standard deviation (Fig. 4). This might be one reason for the lack of significant correlation between  $\text{tpO}_2$  levels and normalized SUV in low-uptake areas. As intratumoral hypoxia is generally considered to result from insufficient oxygen supply paralleling the distance from normal vessels surrounding the tumor, intratumoral oxygen pressure should be higher in more peripheral regions of glioblastoma that are also supplied with blood from normal vessels surrounding the tumor bulk [24, 25]. On PET in the present study, interestingly, high-uptake areas were observed partially within the intermediate layer of enhancing lesions on Gd-T1WI, and low-uptake areas were seen not only in the peripheral layer external to the intermediate layer containing high-uptake areas but also in the inner core layer adjacent to the central necrosis deep to the intermediate layer (Fig. 1b). We assumed that low-uptake areas in both peripheral and inner core layers might contain little  $^{18}\text{F}$ -FRP170-accumulating hypoxic cells, but the peripheral layers included many viable cells at relatively high oxygen pressure, while the inner core comprises low metabolic-hypoxic cells undergoing degenerative apoptosis or necrosis. Remaining low-uptake areas in the intermediate layer probably represent mixture of the two histological types described above. Pistollato et al. [26] evaluated biological characteristics in tissues isolated from three concentric layers (core, intermediate, and peripheral layers) in glioblastoma. The core and intermediate layers showed expression of HIF-1 $\alpha$  as a hypoxic cell marker, whereas the peripheral layer did not express HIF-1 $\alpha$ , but showed expressions of glial fibrillary acidic protein and  $\beta$ -III-tubulin as mature neural cell markers. In addition, core and intermediate layers contained more glioblastoma stem cells, which are well known to be frequently seen in hypoxic niches. These results suggest that inner core and peripheral layers depicted as low-uptake areas on  $^{18}\text{F}$ -FRP170 PET in the present study are likely to exhibit hypoxic and relatively normoxic conditions, respectively.

Hypoxic condition rapidly induces overexpression of HIF-1 $\alpha$  for transcribing target genes such as vascular endothelial growth factor to induce angiogenesis, as countermeasures against hypoxic conditions. Under normoxic conditions, prolyl hydroxylation is induced in HIF-1 $\alpha$ , allowing binding to the von-Hippel-Lindau protein, which mediates ubiquitination of HIF-1 $\alpha$  and subsequent proteasomal degeneration in the cytoplasm. However, under hypoxic conditions, the oxygen requiring prolyl hydroxylase remains inactive, resulting in accumulation of the constitutively expressed HIF-1 $\alpha$  protein in cytoplasm. This subunit is phosphorylated and translocated to the nucleus, where it dimerizes with the HIF-1 $\beta$  subunit, binding to the hypoxia-

response elements upstream of HIF-1-regulated target genes [27]. Therefore, increasingly activated-HIF-1 $\alpha$  induced by hypoxia accumulates in the nucleus. In this study, all specimens obtained from high-uptake areas clearly showed nuclear staining for HIF-1 $\alpha$ , whereas this finding was seen in low-uptake areas in only two patients. Furthermore, mean HIF-1 $\alpha$  staining index determined by the percentage of cells showing nuclear staining was significantly higher in high-uptake areas than in low-uptake areas. Necrotic tissue obtained from a low-uptake area of one patient showed an extremely low HIF-1 $\alpha$  staining index. These findings might support the concept that high-uptake areas represent more hypoxic regions with a high density of viable and active hypoxic cells. Tissues of low-uptake areas were not obtained from deeper than high-uptake areas but rather from the same depth or more externally during surgery in all six patients. As a result, HIF-1 $\alpha$  was also detected in the low-uptake areas of all patients, but showed a greater variety of features than high-uptake areas. These findings support the possibility that low-uptake areas comprised either numerous viable cells under conditions of relatively higher oxygen pressure or low metabolic hypoxic cells under degenerative apoptosis or necrosis.

In the present study, PET at 60 min after intravenous injection of  $^{18}\text{F}$ -FRP170 could provide visually fine-contrast PET images. Shidehara et al. [13] reported fine-contrast color images provided by imaging at 120 min after injection of  $^{18}\text{F}$ -FRP170 in patients with malignant brain tumor. Kaneta et al. [21] reported that imaging results at 120 min after injection of  $^{18}\text{F}$ -FRP170 for patients with lung cancer contributed only a slightly higher tumor/blood ratio when compared with that at 60 min, and concluded that imaging at 60 min after administration was clinically sufficient for assessing hypoxic cells in tumors. The present study supported these recommendations by Kaneta et al. In an experimental study using mice bearing cultured cancer cells,  $^{18}\text{F}$ -FAZA displayed significant higher tumor-to-background ratios compared with  $^{18}\text{F}$ -FMISO and another azomycin-based nucleoside, iodoazomycin arabinoside, labeled with  $^{124}\text{I}$  ( $^{124}\text{I}$ -IAZA), when scanning for all tracer was fixed in 3 h post-injection [28]. Clinically, PET imaging with  $^{18}\text{F}$ -FMISO and  $^{18}\text{F}$ -FAZA has usually been scanned at 120–140 [5–7] and 120–210 min [8] after administration, respectively. Although no previous reports have directly compared  $^{18}\text{F}$ -FRP170 PET and  $^{18}\text{F}$ -FMISO PET images,  $^{18}\text{F}$ -FRP170 PET has been considered superior in terms of fine contrast and rapid clearance from blood [21]. The short duration for imaging could represent an additional advantage to  $^{18}\text{F}$ -FRP170 PET.

Some limitations regarding the interpretation of study results must be considered for this study. First, the sample size in this study was small. Additional studies of a larger number of patients with glioblastoma are needed. Second, use of smaller ROIs might provide more rigorous results in comparisons among SUV,  $\text{tpO}_2$ , and histological features. However, in this study, we placed relatively huge ROIs of

10 mm in diameter to avoid misplacement of microelectrodes within the ROI and sampling error of tumor tissues corresponding to the ROI. These issues could represent factors contributing to make maximum SUV within the ROI unsuitable for use in this study. In short, errors involving differences between pinpoint regions for insertion of electrode and maximum SUV could easily be anticipated. Third, direct  $\text{tpO}_2$  measurements using microelectrodes available differ in sensitivity, accuracy, ability to measure oxygen availability among types of probe used, and impossibility in differentiation between hypoxic and necrotic tissues, although this technique is commonly considered a gold standard [4]. Other techniques indirectly measuring oxygen through reduced drug levels, hemoglobin saturation, or perfusion have been proposed. However, indirect measurements, although valuable, require a set of assumptions to relate the measurement to  $\text{tpO}_2$  or oxygen concentration [4]. Fourth, measurement of  $\text{tpO}_2$  using electrodes in this study did not strictly represent intracellular oxygen pressure, but rather the oxygen pressure of tissue containing hypoxic cells. However,  $\text{tpO}_2$  as measured in this study would correlate with intracellular oxygen pressure, as intracellular oxygen pressure is regulated by extracellular conditions. Fifth, measured  $\text{tpO}_2$  values in this study were relatively higher ( $21.7 \pm 6.2$  mmHg in high-uptake areas and  $40.1 \pm 10.4$  mmHg in low-uptake areas) than in previous reports of direct measurement using Eppendorf oxygen electrodes in malignant brain tumors, where mean  $\text{tpO}_2$  has been reported as approximately  $\leq 20$  mmHg [20, 24, 29]. In particular, mean value in low-uptake areas was significantly higher. However, mean  $\text{tpO}_2$  in low-uptake areas was lower than that of brain tissue around the tumor ( $59.8 \pm 6.5$  mmHg) in a previous report [20]. In previous reports regarding oxygen pressure at high-uptake areas on  $^{18}\text{F}$ -FMISO PET in animal tumor models, measurements using Eppendorf electrodes showed a high frequency of  $\text{tpO}_2 \leq 10$  mmHg [15, 30, 31]. Although the reasons for this contradiction are not entirely clear, we consider these results may have arisen from differences in the electrodes used, or from the inflow of a small amount of air into the trajectory when electrodes were inserted immediately after removal of the navigation marker with a larger diameter than the electrode. However, as this issue applied to measurements of  $\text{tpO}_2$  for all patients in this study, the findings of higher  $\text{tpO}_2$  in high-uptake areas compared to low-uptake areas appear valid.

## Conclusions

Findings of a significant correlation between normalized SUV and  $\text{tpO}_2$ , and strong nuclear immunostaining for HIF-1 $\alpha$  in areas of high  $^{18}\text{F}$ -FRP170 accumulation, suggest that high-uptake areas on  $^{18}\text{F}$ -FRP170 PET represent high densities of viable hypoxic cells, at least in glioblastoma. However, interpretation of low-uptake areas is more complicated, given the likelihood that these lesions comprise

various oxygen environments containing low densities of viable hypoxic cells.

**Acknowledgments.** This study was supported in part by Grant-in-Aid for Strategic Medical Science Research Center for Advanced Medical Science Research from the Ministry of Science, Education, Sports and Culture, Japan.

**Conflict of Interest.** The authors declare that they have no conflicts of interest.

## References

- Jensen RL (2009) Brain tumor hypoxia: tumorigenesis, angiogenesis, imaging, pseudoprogression, and as a therapeutic target. *J Neurooncol* 92:317–335
- Jensen RL (2006) Hypoxia in the tumorigenesis of gliomas and as a potential target for therapeutic measures. *Neurosurg Focus* 20:E24
- Rich JN (2007) Cancer stem cells in radiation resistance. *Cancer Res* 67:8980–8984
- Mendichovszky I, Jackson A (2011) Imaging hypoxia in gliomas. *Br J Radiol* 84(2):S145–S158
- Eschmann SM, Paulsen F, Reimold M et al (2005) Prognostic impact of hypoxia imaging with 18F-misonidazole PET in non-small cell lung cancer and head and neck cancer before radiotherapy. *J Nucl Med* 46:253–260
- Kawai N, Maeda Y, Kudomi N et al (2011) Correlation of biological aggressiveness assessed by 11C-methionine PET and hypoxic burden assessed by 18F-fluoromisonidazole PET in newly diagnosed glioblastoma. *Eur J Nucl Med Mol Imaging* 38:441–450
- Swanson KR, Chakraborty G, Wang CH et al (2009) Complementary but distinct roles for MRI and 18F-fluoromisonidazole PET in the assessment of human glioblastomas. *J Nucl Med* 50:36–44
- Postema EJ, McEwan AJ, Riauka TA et al (2009) Initial results of hypoxia imaging using 1- $\alpha$ -D:-(5-deoxy-5-[<sup>18</sup>F]-fluoroarabino-furanosyl)-2-nitroimidazole (<sup>18</sup>F-FAZA). *Eur J Nucl Med Mol Imaging* 36:1565–1573
- Sheehan JP, Popp B, Monteith S et al (2011) Trans sodium crocetinate: functional neuroimaging studies in a hypoxic brain tumor. *J Neurosurg* 115:749–753
- Tateishi K, Tateishi U, Sato M et al (2013) Application of <sup>62</sup>Cu-diacetyl-bis (N4-methylthiosemicarbazone) PET imaging to predict highly malignant tumor grades and hypoxia-inducible factor-1 $\alpha$  expression in patients with glioma. *AJNR Am J Neuroradiol* 34:92–99
- Kaneta T, Takai Y, Kagaya Y et al (2002) Imaging of ischemic but viable myocardium using a new 18F-labeled 2-nitroimidazole analog, 18F-FRP170. *J Nucl Med* 43:109–116
- Ishikawa Y, Iwata R, Furumoto S, Takai Y (2005) Automated preparation of hypoxic cell marker [<sup>18</sup>F]FRP-170 by on-column hydrolysis. *Appl Radiat Isot* 62:705–710
- Shibahara I, Kumabe T, Kanamori M et al (2010) Imaging of hypoxic lesions in patients with gliomas by using positron emission tomography with 1-(2-[<sup>18</sup>F] fluoro-1-[hydroxymethyl]ethoxy)methyl-2-nitroimidazole, a new 18F-labeled 2-nitroimidazole analog. *J Neurosurg* 113:358–368
- Matsumoto K, Szajek L, Krishna MC et al (2007) The influence of tumor oxygenation on hypoxia imaging in murine squamous cell carcinoma using [<sup>64</sup>Cu]Cu-ATSM or [<sup>18</sup>F]Fluoromisonidazole positron emission tomography. *Int J Oncol* 30:873–881
- Sorensen M, Horsman MR, Cumming P et al (2005) Effect of intratumoral heterogeneity in oxygenation status on FMISO PET, autoradiography, and electrode Po<sub>2</sub> measurements in murine tumors. *Int J Radiat Oncol Biol Phys* 62:854–861
- Mahy P, De Bast M, Gallez B et al (2003) In vivo colocalization of 2-nitroimidazole EF5 fluorescence intensity and electron paramagnetic resonance oximetry in mouse tumors. *Radiother Oncol* 67:53–61
- Tran LB, Bol A, Labar D et al (2012) Hypoxia imaging with the nitroimidazole <sup>18</sup>F-FAZA PET tracer: a comparison with OxyLite, EPR oximetry and 19F-MRI relaxometry. *Radiother Oncol* 105:29–35
- Wang GL, Semenza GL (1995) Purification and characterization of hypoxia-inducible factor 1. *J Biol Chem* 270:1230–1237
- Collingridge DR, Piepmeyer JM, Rockwell S, Knisely JP (1999) Polarographic measurements of oxygen tension in human glioma and surrounding peritumoural brain tissue. *Radiother Oncol* 53:127–131
- Kayama T, Yoshimoto T, Fujimoto S, Sakurai Y (1991) Intratumoral oxygen pressure in malignant brain tumor. *J Neurosurg* 74:55–59
- Kaneta T, Takai Y, Iwata R et al (2007) Initial evaluation of dynamic human imaging using <sup>18</sup>F-FRP170 as a new PET tracer for imaging hypoxia. *Ann Nucl Med* 21:101–107
- Chapman JD (1979) Hypoxic sensitizers—implications for radiation therapy. *N Engl J Med* 301:1429–1432
- Krohn KA, Link JM, Mason RP (2008) Molecular imaging of hypoxia. *J Nucl Med* 49(Suppl 2):129S–148S
- Beppu T, Kamada K, Yoshida Y et al (2002) Change of oxygen pressure in glioblastoma tissue under various conditions. *J Neurooncol* 58:47–52
- Brown JM (1979) Evidence for acutely hypoxic cells in mouse tumours, and a possible mechanism of reoxygenation. *Br J Radiol* 52:650–656
- Pistollato F, Abbadi S, Rampazzo E et al (2010) Intratumoral hypoxic gradient drives stem cells distribution and MGMT expression in glioblastoma. *Stem Cells* 28:851–862
- Fischer I, Gagner JP, Law M, Newcomb EW, Zagzag D (2005) Angiogenesis in gliomas: biology and molecular pathophysiology. *Brain Pathol* 15:297–310
- Reischl G, Dorow DS, Cullinane C et al (2007) Imaging of tumor hypoxia with [<sup>124</sup>I]IAZA in comparison with [<sup>18</sup>F]FMISO and [<sup>18</sup>F]FAZA—first small animal PET results. *J Pharm Pharm Sci* 10:203–211
- Rampling R, Cruickshank G, Lewis AD et al (1994) Direct measurement of pO<sub>2</sub> distribution and bioreductive enzymes in human malignant brain tumors. *Int J Radiat Oncol Biol Phys* 29:427–431
- Piert M, Machulla H, Becker G et al (1999) Introducing fluorine-18 fluoromisonidazole positron emission tomography for the localisation and quantification of pig liver hypoxia. *Eur J Nucl Med* 26:95–109
- Bartlett RM, Beattie BJ, Naryanan M et al (2012) Image-guided PO<sub>2</sub> probe measurements correlated with parametric images derived from <sup>18</sup>F-fluoromisonidazole small-animal PET data in rats. *J Nucl Med* 53:1608–1615